THE ASTROPHYSICAL JOURNAL, 410:574–585, 1993 June 20

THE INTERACTING SYSTEM NGC 7753–7752 (ARP 86). I. *BVRI* PHOTOMETRY

EIJA LAURIKAINEN
Tuorla Observatory, University of Turku, SF-21500 Piikkiö, Finland
HEIKKI SALO
Department of Astronomy, University of Oulu, SF-90570 Oulu, Finland
AND
ANTONIO APARICIO
Instituto de Astrofisica de Canarias, Via Lactea, E-38200 La Laguna, Tenerife, Canary Islands, Spain
Received 1992 September 8; accepted 1992 December 17

ABSTRACT

BVRI surface photometry is presented for the interacting galaxy pair Arp 86 (NGC 7753–7752). Deep, high-resolution images were obtained in order to study the faint tidal features. The bridge was found to be bluer than the tail both in $V-R$ and $B-V$, the $V-R$ color probably suggesting enhanced long-term star formation in the bridge. The end of the bridge is extremely blue in $B-V$ (0.2–0.4), thus indicating present ongoing star formation. The CCD images were also used to estimate initial parameters, such as inclinations and disk scale lengths for the dynamical modeling of Arp 86, presented in Salo & Laurikainen (1993).

Subject headings: galaxies: individual (NGC 7753–7752) — galaxies: interactions — galaxies: photometry — galaxies: structure

1. INTRODUCTION

Arp 86 is an M51-type object consisting of a main galaxy and a small companion at the tip of one of the arms. Companions of this kind of pairs are often irregular objects comparable to the brightest irregular field galaxies or, alternatively, nearly round and compact objects of high surface brightness (Vorontsov-Vel'yaminov 1976), NGC 7752 belonging to the latter group as noticed by Petrov (1986). M51-type objects are so numerous that the apparent location of the companions at the end of the main galaxy spiral arm can hardly be just a random projection effect (Vorontsov-Vel'yaminov 1958). Like M51, NGC 7753 is a grand-design galaxy with bright, disk-dominating spiral arms.

Several explanations for the origin of M51-type objects have been suggested. For example, (1) Zwicky proposed in 1956 that collisions between giant galaxies eject matter to intergalactic space, out of which dwarf galaxies may form. Incidentally, this hypothesis has recently been explored by Mirabel, Dottori, & Lutz (1992) for the case of NGC 4038/4039. (2) Arp's suggestion in 1969 was that companions were ejected some 10^7–10^8 yr ago from parent galaxies, being short-lived because of their internal ejection processes. According to Arp (1969), NGC 7752 should now be in the ejection phase, the knotty central appearance being produced by material ejected from its own nucleus, which would disrupt the companion galaxy in about 10^7 yr. (3) Since the test-particle simulations of Toomre & Toomre (1972), it has been generally accepted that gravitational interactions are responsible for several types of peculiar morphologies. In particular, Toomre & Toomre applied their tidal hypothesis to the M51 system, and demonstrated the formation of tail and bridge structures, although they failed to reproduce the inner strong spiral pattern. Moreover, in the classical view of near-parabolic encounters (Toomre & Toomre 1972; Hernquist 1990) it is difficult to explain why so many companions appear at the tip of the bridge arms.

Grand-design galaxies are in general found to be slightly brighter than flocculent galaxies; on the other hand, star formation rate per unit area is independent of arm class (Elmegreen & Elmegreen 1987). Therefore, it appears that star formation in density waves does not dominate the global star formation. Although it is not known whether the same holds for tidally induced spiral arms, this seems to be in agreement with the result that colors of the tidal features are similar to those of most interacting galaxies, the tidal features thus interpreted to be stripped material from the disk (Schombert, Wallin, & Struck-Marcell 1990). Nevertheless, there is evidence that in some galaxies tidal tails and bridges are so blue that ongoing star formation must be occurring (Schombert et al. 1990).

In the present investigation we determine the observational initial parameters for dynamical modeling of Arp 86, presented in Salo & Laurikainen (1993, hereafter Paper II), as well as surface photometry in order to study the star-forming locations. Mildly disturbed pairs with a small perturber form an interesting subclass of interacting galaxies, as in this case the perturbations lead to rather modest but still long-lasting tidal features. In this case rather accurate dynamical modeling is expected to be possible, in contrast to strongly disturbed systems or mergers, where the estimation of the initial parameters is very difficult. This kind of observational and dynamical project has been started, with the goal of correlating the strength and duration of the perturbation with the induced star formation rate and nuclear activity. M51-type galaxies, of which Arp 86 is a good example, form an important subclass of close, but still not too perturbed, objects.

2.. OBSERVATIONS

The observational data for Arp 86 were obtained at the 2.5 m Nordic Optical Telescope (La Palma) in 1991 July, and at the 1.5 m telescope of the Observatorio Astronómico National (Calar Alto) in 1991 August. The 2.5 m telescope was equipped with a Tektronix 512 × 512 CCD chip, with pixel size of 0".2. The 1024 × 1024 pixel CCD at the 1.5 m telescope had a pixel size of 0".32.

The 2.5 m telescope was used to obtain a deep, high-

resolution image in the Gunn R band, in which wavelength region the quantum efficiency of the CCD was highest. Since the field size was only 100″, seven separate fields of Arp 86 were observed, with an overlap of one-quarter of the field size, in order to have enough stellar identifications to superpose the images. In each field two 15 minute integrations were performed. The mosaic, shown in Figure 1 (in digital units and in linear scale) was constructed using the IDL data processing package (Research System, Inc.). In Figure 1 only the disk area of the main galaxy is shown, in order to demonstrate its fine structure. Several stellar positions in each overlapping region were measured, by fitting Gaussians to stellar flux profiles, and these measurements were then used to superpose the images. The 1.5 m telescope data were used for photometry in the Johnson B, V, R, and I bands (the images are shown in Fig. 2). The total integration time was 1 hr in every band, but because of problems with dust features in the images, the useful times were reduced to 30 minutes in the B, V, and I bands. In Calar Alto the weather conditions were photometric, and the seeing varied between 1″.5 and 2″.0, of which about one-half was due to the dome conditions. In La Palma there was some Sahara dust in the air, but the seeing was excellent, being typically between 0″.6 and 0″.7.

The images were processed with Sun workstations at the Astronomy Department of Oulu University (Finland) and the Instituto de Astrofisica de Canarias (Spain) in IRAF and IDL environments. Preliminary reductions were made by using standard procedures for bias and dark subtraction and flat-fielding (a series of twilight flat fields were obtained every night in each band). The cosmic rays were eliminated locally, using IRAF and IDL procedures. Since accurate flat-fielding was essential, the remaining small gradients in the images were eliminated by bilinear interpolation using the IMSURFIT program of IRAF. After this correction, the gradients in the 2.5 m data were not more than 1 analog to digital converter unit (ADU), or about 25% of the sky noise, and in the 1.5 m images they were also below the noise level (except in the I-band image). Some of the 1.5 m images needed additional care, owing to dust and charge-transfer problems which could not be corrected by normal calibration procedures. For some reason unknown to us, the signal levels of the images dropped by 1–5 ADU following the exposure to bright, unsaturated objects. This defect was corrected by adding a constant to parts of the images with lowered ADU levels as compared with adjacent columns. The gradients produced in this procedure were corrected by interpolation methods. The dust problem in some of the images was not possible to resolve, and these images were discarded. The dust features varied during each night, probably because of interference effects between the dust in the chip and in the filter wheel. The noise levels of the sky background in the reduced images in the 2.5 m data were 4.0 ADU, and in the 1.5 m data 1–1.4 ADU in the B, V, and R

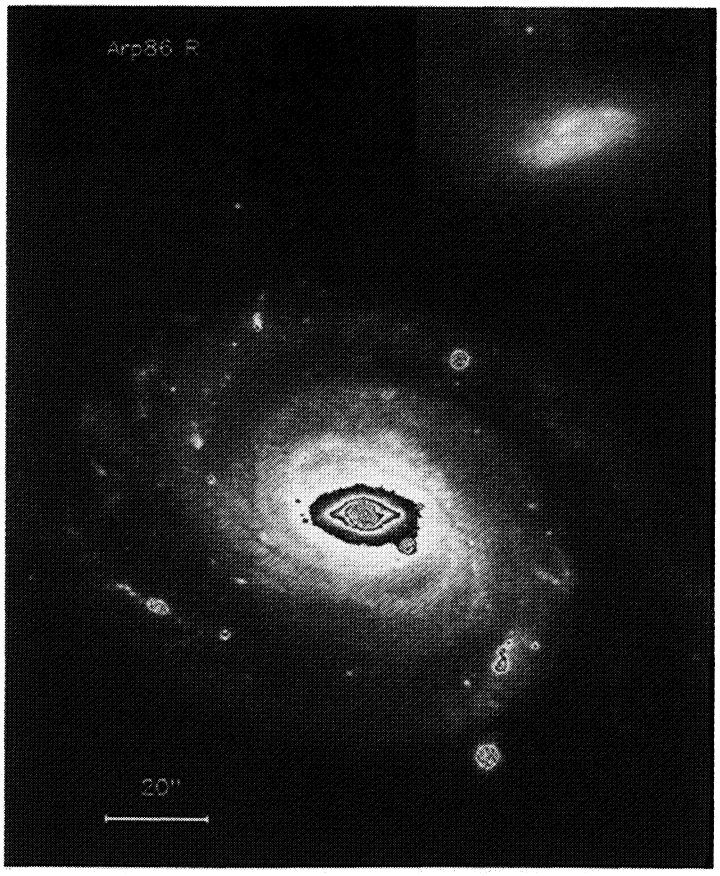

FIG. 1.—Cleaned R image obtained at the Nordic Optical Telescope. The image is a mosaic of seven different fields. Here only a portion of the main galaxy is displayed in order to better show the local morphology of the inner regions. The inset displays the companion, on the same scale.

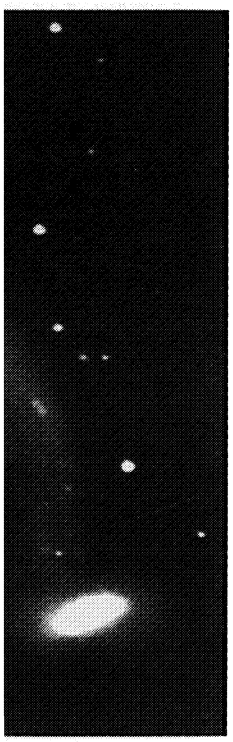

d in Calar Alto

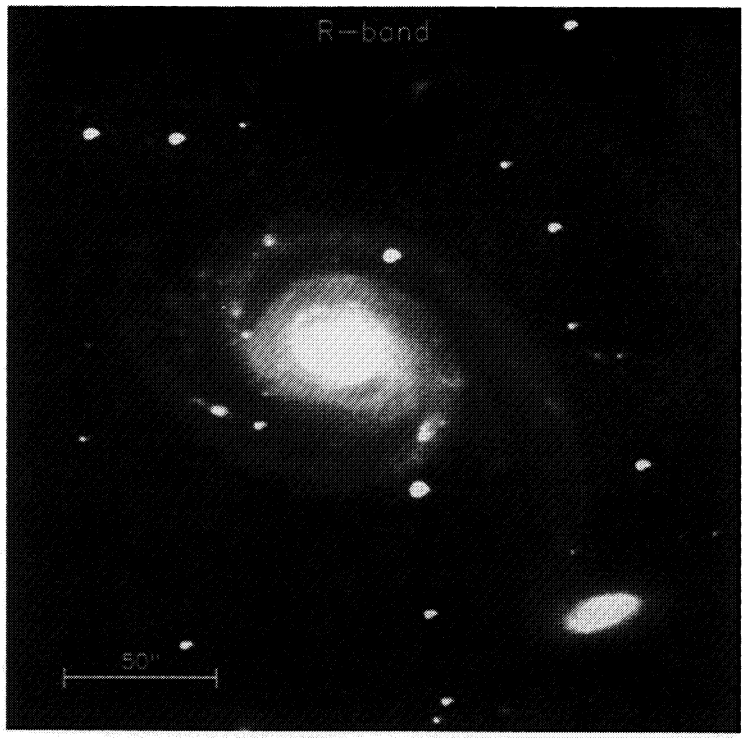

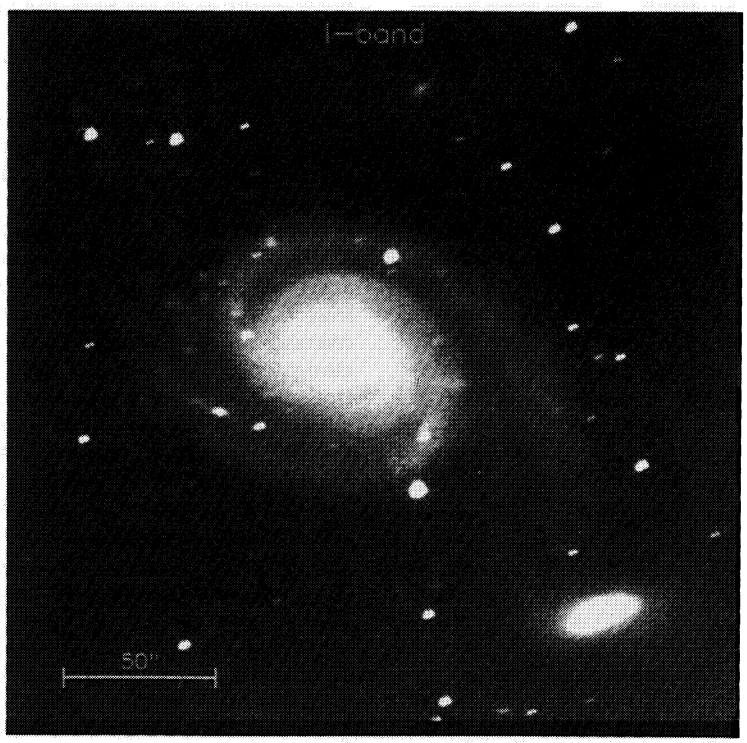

FIG. 2—*Continued*

bands and 13.6 ADU in the I band. The quality of the I image was not comparable to that of the other images, and it will be used with caution in the following analysis.

The photometric calibration of the 1.5 m images was performed using the standard stars from Landolt (1983), seven to 10 standard stars being observed every night in each band. The observed images were converted to magnitude scale by transforming the instrumental magnitudes to the Johnson system, so that the standards of all five nights of the observing run were used. Proper extinction for each night was applied. The total errors of the magnitude calibration were less than 0.04 mag. Since these observations are part of a larger observing run, the flux calibration is explained in more detail in a forthcoming paper by Laurikainen & Aparicio (1993). Accepting the pixel values larger than 3 σ above the sky level, our magnitudes are valid to the limit of 25.5 mag arcsec^{-2}.

3. ANALYSIS

3.1. *Morphology*

NGC 7753 is classified as SAB(*rs*)bc by de Vaucouleurs, de Vaucouleurs, & Corwin (1976), and as SAB(*rs*)b by Nilson (1973). The spiral arms of the main galaxy are rather symmetric, broad, and long, and they continue deep into the disk. The spiral arms are prominent in the whole optical region, not only in the blue, thus indicating that recent star formation is not the principal reason for their brightness, being rather true density variations in origin.

The strengths of the density waves have been estimated by measuring the intensity profiles across the two main spiral arms, defining the strength as the difference between the minimum intensity in the interarm region and the maximum intensity in the arm. We found that the contrast is very strong in the bridge, being 0.6 mag (30% amplitude) in points 28–30 in Figure 9, and that the strength decreases from the edge of the galaxy toward the inner disk. In the tail the intensity variation is only 0.1 mag (5% amplitude) in points 4–7 (Fig. 9).

In spite of the rather symmetric morphological structure, NGC 7753 shows some peculiarities. For example, the bridge looks longer than the tail and is also brighter. Figure 3 demonstrates the extent of the weakest regions in the R band down to the intensity level of 3 σ above the sky level, showing that at low intensity levels the arms are equally broad and long. At the end of the tail there is a large material condensation visible only at low ADU levels, which, although not a dominant feature in NGC 7753, is interesting in relation to the interpretation of the dynamical history of the galaxy (to be discussed in Paper II). Additionally, NGC 7753 has two secondary, very weak spiral extensions which have no continuity in the disk.

The distribution and local morphology of star-forming regions vary along the spiral features. At the end of the bridge (points 21–26 in Fig. 9) they have clumpy appearance and are located in both branches of the broken double arm (see inset in Fig 1, showing the bridge in the vicinity of the companion). Farther inward along the bridge the stellar associations are concentrated to the concave edge of the arm (points 26–31), whereas in points 34–45 in the bridge, and in points 9–20 in the tail, the associations are distributed over the whole arm width. Additionally, there are some giant star-forming regions, perhaps including those at the concave edge of the tail arm, which do not accurately follow the spiral patterns. Some of them (the southwest and northeast directions) have morphologies, such as arcs or chains, sometimes suggested to be associated with stochastic star-forming regions. In the innermost disk (within the 40″) the regular grand-design spiral structure is transformed to a more irregular multiarm system showing signs of dust lanes as well as possible central oval structure.

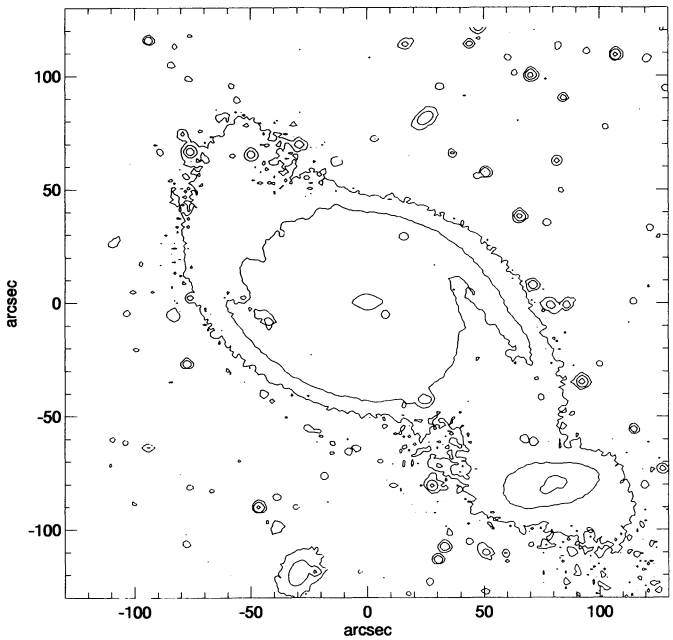

FIG. 3.—Contour plot of the R image, displaying low ADU levels. The minimum intensity level is 3 σ above the sky level.

The companion galaxy NGC 7752 is classified as an Irr galaxy by Nilson (1973). The structure is very irregular within the inner 20″ in all the observed bands.

3.2. *Disk Orientations and Scale Lengths*

Although the interaction is likely to warp the outer parts of the components, the inner disks should more or less retain their initial orientations. In their study of the Arp 86 velocity field Marcelin et al. (1987) adopt inclination $i = 52°$ and position angle P.A. = 53° for the disk of NGC 7753. While the position angle is well determined by the zero velocity line for the 10″–30″ region (excluding the inner oval and outer tidally deformed regions), the inclination is probably overestimated. Indeed, it corresponds to an axial ratio of 0.62, taken from overexposed photographs where the galaxy appears artificially elongated due to tidal features. In order to check the inclination estimate, we made several trials by deprojecting the R-band image by assuming various inclinations between 20° and 60° (Fig. 4). As can be seen, $i \approx 30°$–$40°$ yields the most regular inclination-corrected appearance. The revised value for inclination is further supported by the implied form of the spiral structure: only for $i \approx 40°$ do the inner spirals trace a smooth logarithmic pattern without any special behavior near the apparent major axis (see Fig. 5). Therefore, we adopted the inclination value $i = 40°$. From Figure 5 we also see that the opening angles for the bridge (excluding the part near the companion) and the tail are about 12° and 10°, respectively.

The scale lengths were determined from the I-band image, since it is most likely to represent the old stellar populations where most of the disk mass resides. Figure 6*a* displays the intensity distribution in the I image of the primary component, deprojected to face-on viewing angle. The intensity profile was measured within circular annuli in steps of 2″. The intensity

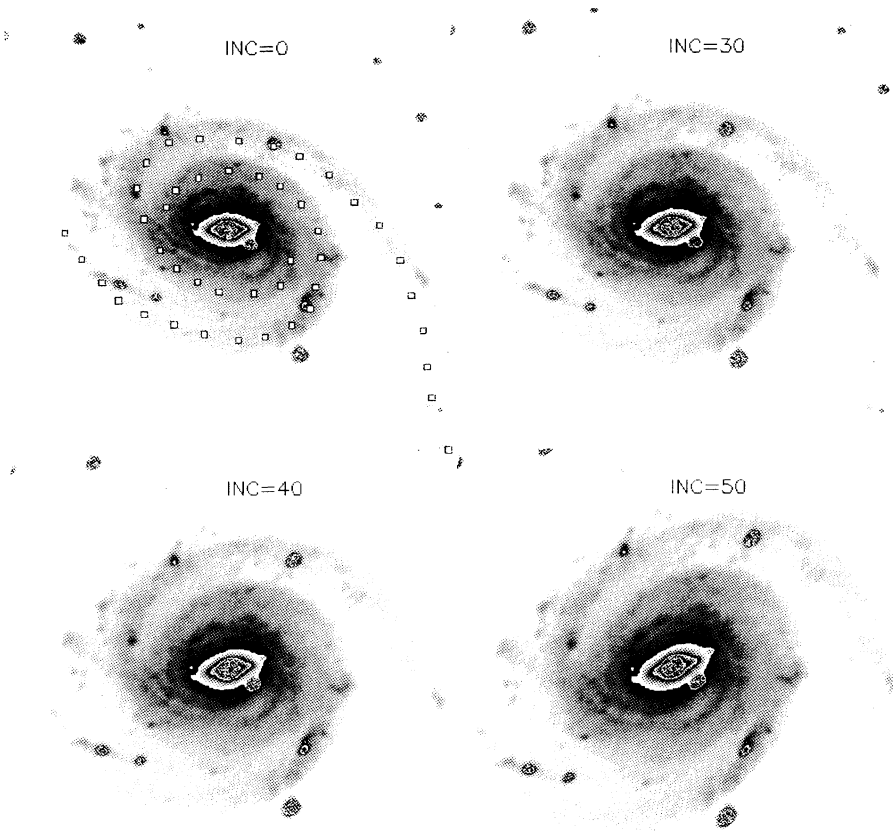

FIG. 4.—Deprojected V image of NGC 7753 for inclinations $i = 0°$, 30°,40°, 50°, and position angle P.A. = 53°. The open squares trace the main observed spiral arms.

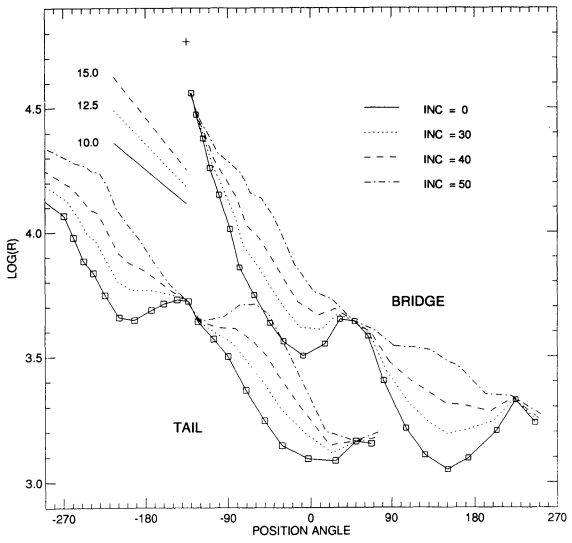

FIG. 5.—Inclination-corrected spiral features of NGC 7753 (traced from V band image), displayed in (ϕ, log R) coordinates, where R is the distance from the center (arcsec) and ϕ is the angle measured from the north. The major-axis position angle is taken to be P.A. = 53°. Various values of disk inclination are studied, assuming that all features are in the same plane. The measured points are those marked by squares in Fig. 4 and are shown by the same symbols for $i = 0°$, while the cross marks the apparent location of the companion. Lines indicate constant slopes for $m = 2$ logarithmic spirals, $\log R = -m/p(\phi - \phi_0)$, with pitch angle $\tan^{-1}(m/p)$.

drops exponentially over the range 15″–60″ with scale length of about 20″. Inside 15″, the bulge follows closely the $R^{1/4}$ law, while outside 60″–70″ the intensity drops more rapidly than predicted by the exponential model. Weak global inhomogeneity of the sky background in the I image does not affect the determination of the scale length, which was confirmed by obtaining the same result from the R image.

The I-band intensity distribution for the companion (Fig. 6*b*) is also consistent with an exponential disk, with a scale length of 3.″7 for the radius in the range 5″–15″. However, inside 5″ the intensity levels off, and outside 15″ it falls less rapidly than the exponential model would imply. The exponential part of the disk covers approximately the clumpy area of the galaxy showing signs of strong star formation (compare with Fig. 7). At the other wavelengths the behavior is similar, although the exponential scale length is slightly reduced for shorter wavelengths (3.″1 in B). It is worth noticing that, while the intensity maintains a constant level after a distance of about 35″ from the galaxy center, the intensity in the V, R, and I bands does not drop to zero. This is probably because at the edge of the galaxy we are also integrating some fraction of the main galaxy brightness.

Constant, positive ADU level at the edge of the galaxy is not an effect of bad sky subtraction, being clearly above the error limits (see Fig. 6*b*). We suppose that the largest source of error is due to nonuniform sky background level in the images, since the instrumental errors are very small. Therefore, the errors were estimated by measuring the sky background level at several points near the galaxy, the dispersion of these measurements giving the flux errors.

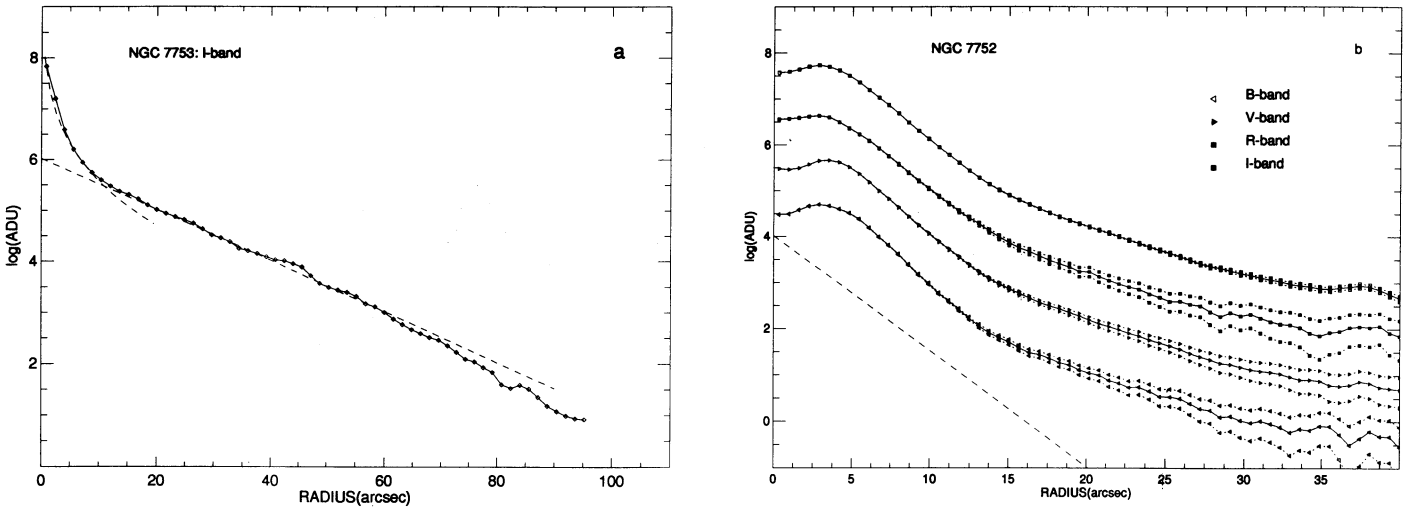

FIG. 6.—Azimuthally averaged intensity profiles (*a*) for NGC 7753 determined from the deprojected *I* image and (*b*) for NGC 7752 from deprojected *B*, *V*, *R*, and *I* images. NGC 7753 was deprojected by assuming P.A. = 53° and $i = 40°$, and NGC 7752 by assuming P.A. = 105° and $i = 55°$. Measurements were made in steps of 2″. Dashed lines indicate exponential models with scale lengths of 20″ for NGC 7753 and 4″ for NGC 7752. For the main disk, an $R^{1/4}$ bulge fit is also displayed. The error bounds indicated by dotted lines for NGC 7752 were determined by measuring the sky level in several directions around the galaxy and estimating the minimum and maximum background value to be subtracted from the dispersion of these sky levels around their mean value. For NGC 7753 this effect is negligible.

The anomalous drop in the intensity profile near the nucleus is probably affected by absorption of dust, probably being related to the strong ongoing star formation visible in the Hα image obtained by Marcelin et al. (1987). The extended envelope might be caused by tidal expansion of the original disk, or the excess material may have originated from the main galaxy.

3.3. *Color Index Maps*

In order to study the stellar population variations between different parts of Arp 86, color index maps in $B-V$, $B-R$, and $V-R$ were constructed (see Fig. 8 [Pl. 4]). Since this kind of study is very sensitive to global gradients, the *I* image was excluded. The original images were first normalized to the

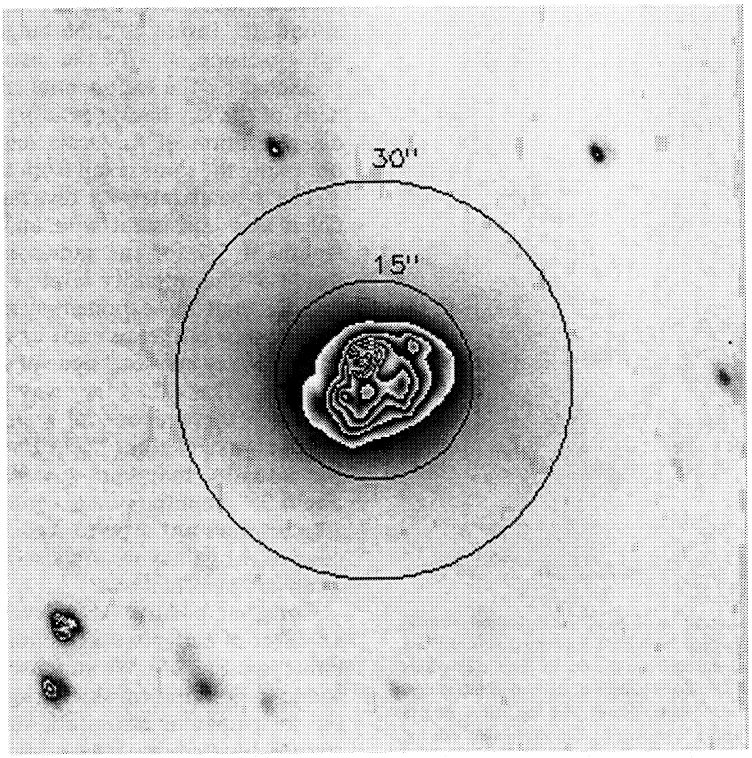

FIG. 7.—NGC 7752 shown in the *R* band, deprojected to face-on position. The inner circle marks the exponential part of the disk intensity profile, extending to the radius of 15″. The circle with radius $R = 30''$ indicates the distance where the intensity profiles start leveling off to a constant value.

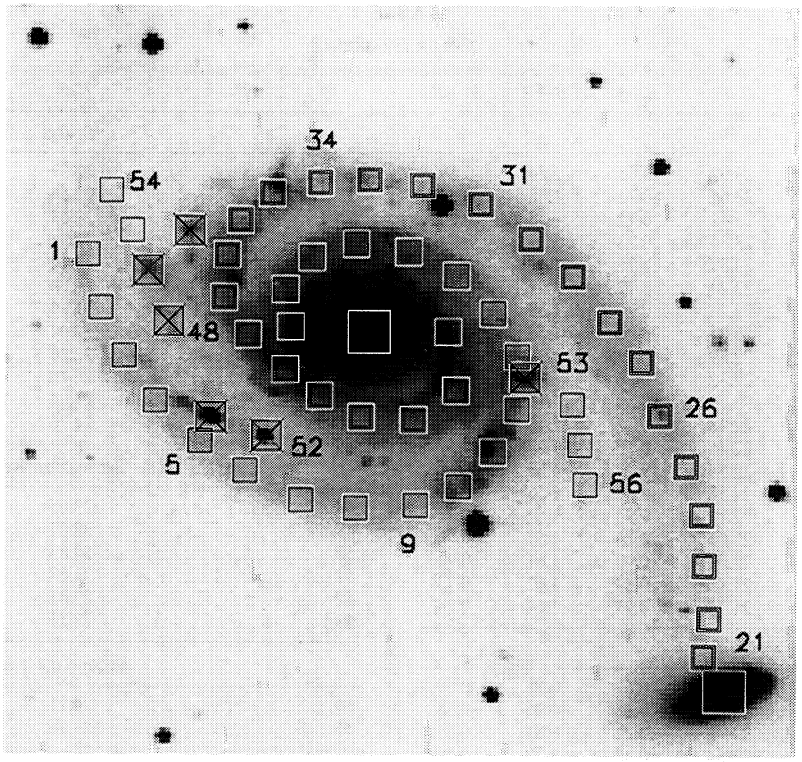

FIG. 9.—Positions of the color measurements are displayed, the bridge and tail locations being marked with different symbols. The boxes with crosses indicate the locations of strong star-forming regions.

same integration time, and to obtain higher signal-to-noise ratio they were rebinned by a 4 × 4 box, which yields a pixel size of 1".32 × 1".32. Colors along the spiral arms of NGC 7753 were measured using rectangular regions, the positions and sizes being displayed in Figure 9, while the color index values and V surface brightnesses are shown in Table 1. While measuring the fluxes, integrations above 3 σ of the sky level were applied, after which the fluxes were converted to the magnitude scale and the color indices were calculated. By measuring the fluxes in ADU instead of magnitudes, low pixel values are not overemphasized.

The instrumental errors estimated from the Poisson noise were smaller than 0.1 mag in $B-V$ and $B-R$, and smaller than 0.04 in $V-R$ (see Fig. 10*b*). The errors decrease exponentially as a function of the surface brightness, whereas the standard deviations of the mean colors are large (see Fig. 10*a*). Because the dispersion is largest in $B-V$ and $B-R$, one would expect that it is mainly caused by the B image, where the ADU

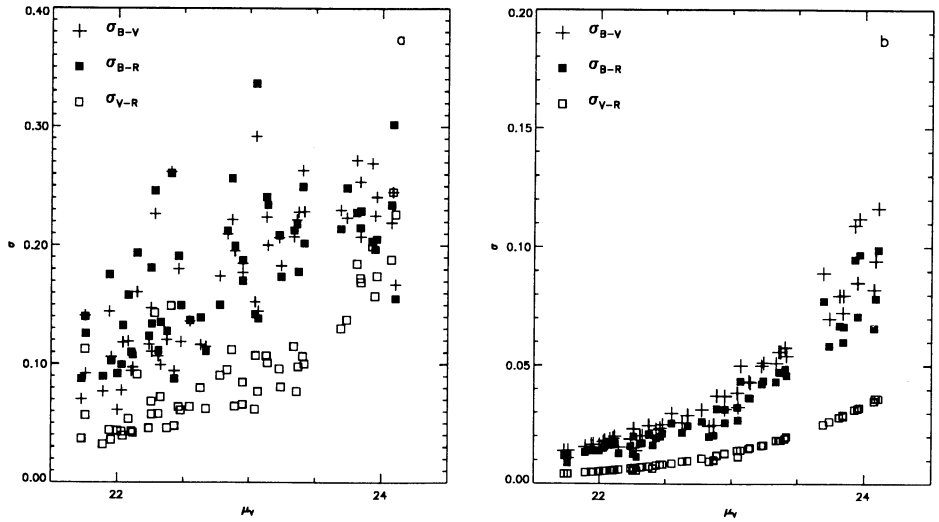

FIG. 10.—Error estimates for color measurements. (*a*) Standard deviations of the mean colors are shown as a function of the surface brightness in the V band. (*b*) Poisson noise is displayed in the same measured positions.

TABLE 1

COLOR GRADIENTS

N[a]	μ[b]	B−V	B−R	V−R
Tail				
1	23.93	0.65	1.24	0.59
2	23.69	0.74	1.38	0.64
3	23.41	0.74	1.38	0.64
4	23.36	0.73	1.37	0.64
5	23.37	0.73	1.42	0.68
6	23.24	0.77	1.41	0.64
7	23.23	0.74	1.39	0.65
8	23.07	0.96	1.56	0.60
9	22.89	0.79	1.39	0.60
10	22.32	0.66	1.21	0.55
11	21.76	0.50	1.14	0.64
12	22.48	0.77	1.40	0.63
13	22.46	0.70	1.27	0.57
14	22.55	0.93	1.62	0.69
15	22.38	0.89	1.58	0.69
16	22.12	0.93	1.64	0.71
17	22.03	0.86	1.57	0.70
18	22.08	0.90	1.61	0.71
19	21.95	0.89	1.62	0.73
20	21.73	0.91	1.64	0.74
Bridge				
21	23.13	0.67	0.78	0.59
22	24.07	0.18	0.76	0.58
23	24.08	0.27	0.81	0.55
24	23.84	0.30	0.79	0.50
25	23.74	0.47	1.02	0.55
26	22.95	0.45	1.00	0.54
27	23.42	0.55	1.05	0.51
28	23.34	0.65	1.14	0.50
29	23.14	0.64	1.16	0.51
30	23.05	0.63	1.13	0.51
31	22.95	0.70	1.23	0.53
32	22.78	0.69	1.28	0.59
33	22.63	0.62	1.17	0.55
Bridge				
34	22.67	0.72	1.34	0.61
35	22.15	0.50	1.09	0.59
36	22.43	0.70	1.29	0.58
37	22.31	0.69	1.29	0.61
38	22.24	0.68	1.30	0.63
39	22.00	0.80	1.47	0.66
40	21.89	0.86	1.58	0.72
41	22.04	0.90	1.61	0.71
42	22.26	0.95	1.68	0.72
43	22.10	0.89	1.63	0.74
44	21.94	0.88	1.62	0.74
45	21.76	0.88	1.62	0.74
Star Formation Regions				
48	23.05	0.61	1.27	0.66
49	22.87	0.46	0.97	0.51
50	22.83	0.45	1.05	0.60
51	22.28	0.42	1.12	0.70
52	22.41	0.72	1.29	0.57
53	22.26	0.56	1.10	0.54
Secondary Tail				
54	24.11	0.58	1.22	0.72
55	23.96	0.63	1.29	0.64
Secondary Bridge				
56	23.95	0.45	1.04	0.58
57	23.84	0.58	1.16	0.63
58	23.81	0.63	1.22	0.59
Nuclei				
NGC 7752	20.33	0.59	1.25	0.66
NGC 7753	20.09	1.11	1.94	0.83

[a] Numbers correspond to locations marked in Fig. 9.
[b] V-band surface brightness in mag arcsec^{-2}.

levels are low; however, the dispersion is similar in every band. This, together with the fact that the dispersion depends very little on the surface brightness, implies that part of the color dispersion must reflect real stellar population variations within each measurement area.

The results for the spiral arms of NGC 7753 are displayed in Figure 11, where the diametrically opposite points of the bridge and the tail are shown in the same abscissa positions. Within the inner 20″–25″ from the center, the bridge and the tail have the same $B-V$ colors (points 14–20 and 40–45 in Fig. 11*a*), the mean $B-V$ value being 0.9 mag. Outward from this distance the bridge is bluer and brighter than the tail (see Fig. 11*d*). The end of the bridge, which is broken into two arms (indicated by the arrow) is very blue in $B-V$ (0.2–0.4; see Fig. 11*a*), as blue as the bluest colors found by Schombert et al. (1990) for tidal features of interacting galaxies in their sample, thus indicating ongoing star formation in the bridge. The large dispersion in the zone marked by a horizontal dashed line in Figure 11 is caused by clumpiness of star-forming regions there, and the red color in the measured point 21 is due to the contribution of the NGC 7752 stellar population.

The bridge and the tail have similar $V-R$ color gradients in the disk up to the measured points 33 and 8 (Fig. 11*c*). The tidal tail is redder than the outer disk, whereas the bridge continues to become bluer toward the edge of the galaxy up to the broken part of the arm (point 26), where it turns redder again. The disk $V-R$ gradient can be understood by the decreasing contribution of old bulge stars toward the edge together with differential reddening, but the color differences between the tidal arms are difficult to explain only by undisturbed evolution of the galaxy. The very red $V-R$ color of the tidal tail most probably is not caused by Hα emission lines in the R band, because the measured points have no visible star-forming regions. One possible explanation is that massive stars were induced tidally a long time ago in the tail, which stars have since then rapidly evolved. Another possibility is that the tail material originates from deeper inside the main galaxy than the bridge material, but from the dynamical point of view there is little evidence for this interpretation. The long $V-R$ gradient toward the blue in the bridge could be understood if the bridge was continuously disturbed. There may be a continuous stripping in progress, transporting disk gas toward the companion with a follow-up of star formation, and the gradient may be a manifestation of an age effect in the bridge. On the other hand, the end of the bridge is very clumpy, consisting of large young stellar associations, so that part of its very red color may be caused by Hα lines in the R band or may be due to red giant stars instead of a large contribution of the old

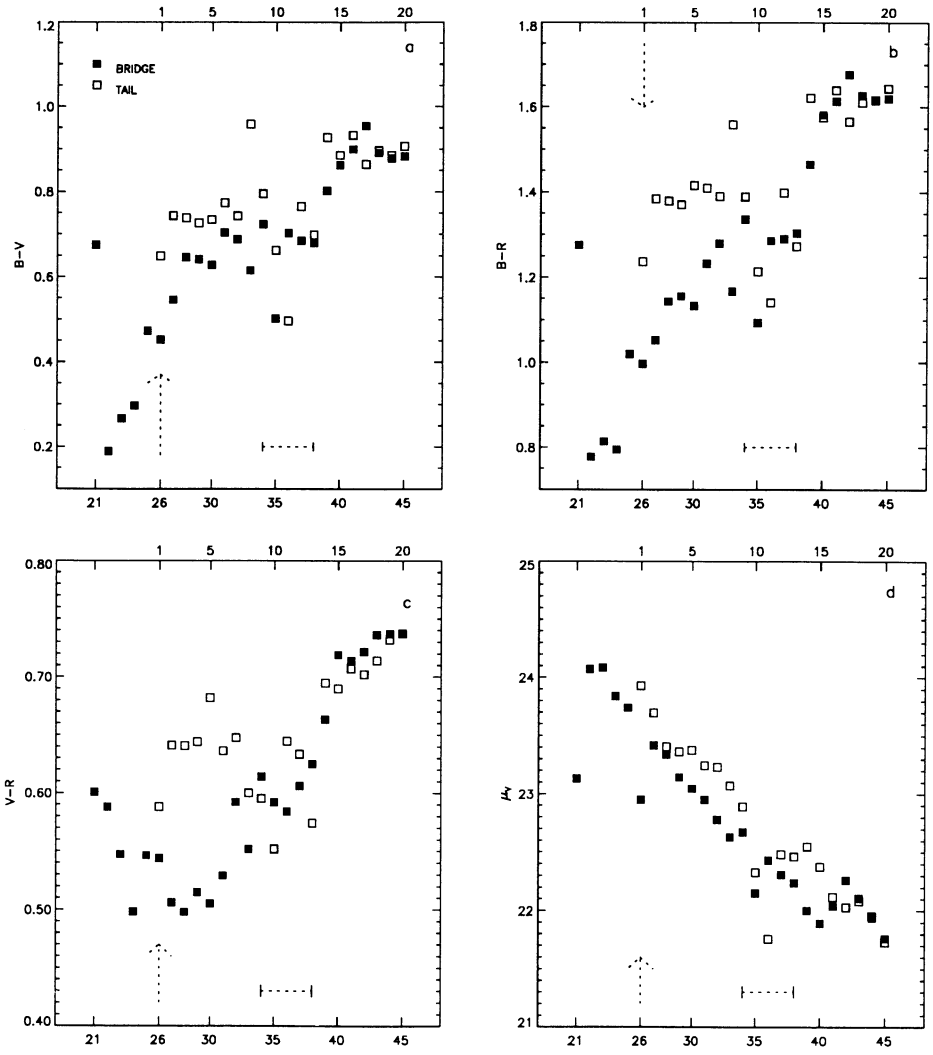

FIG. 11.—Colors (*a*) $B-V$, (*b*) $B-R$, and (*c*) $V-R$, as well as (*d*) surface brightness in the V band, are shown along the bridge and the tail. Radial distance decreases to the right. The numbers on the x-axis correspond to the locations shown in Fig. 9 (tail measurements at the upper and bridge at the lower x-axis). The point 26, indicated by a dashed arrow, is the turning point, where the double arm of the bridge begins, and the colors rapidly change. The vertical dashed lines indicate the locations of clumpy star-forming regions in the spiral arms.

stellar population. The $V-R$ colors of the bridge very near to the companion (points 21–22) are close to the colors obtained for the companion galaxy, so that they are most probably affected by the extended overlapping stellar disk of the companion.

The colors for the nucleus of NGC 7752 are $B-V = 0.59$, $B-R = 1.25$, and $V-R = 0.66$. Although these colors are blue, they are redder than the end of the bridge, probably due to large extinction in the companion galaxy. Indeed, if we adopt the extinction correction $E(B-V) = 0.72$, measured by Laurikainen & Moles (1989) and use the transformation between the colors following Savage & Mathis (1979), the colors will be reduced to $B-V = 0.12$, $B-R = 0.0$, and $V-R = 0.10$. Galactic extinction, using the values obtained from Burstein & Heiles (1982, 1984) is 0.007 in $B-V$, 0.011 in $B-R$, and 0.005 in $V-R$. The internal extinction correction derived was only approximate, owing to the problem of Balmer absorption lines in the emission spectrum, and owing to the fact that it might be strongly variable inside the galaxy. In any case, the extinction-corrected colors show that NGC 7752 is extremely blue with strong star formation processes in progress. In fact, allowing for possible inaccuracy in the extinction estimate, the colors seem to be consistent with colors of H II regions as given in Larson & Tinsley (1978).

We also estimated the total magnitudes for Arp 86. The fluxes were integrated by eliminating the stars and excluding the contribution of the galactic bridge for the companion. The obtained magnitudes for NGC 7753 are $B = 13.01$, $V = 12.12$, and $R = 11.43$, and for NGC 7752, $B = 14.72$, $V = 14.14$, and $R = 13.49$. The errors, including photometric and instrumental errors, are 0.043 for NGC 7753 and 0.041 for NGC 7752. The obtained B-magnitudes are close to the photographic magnitudes 13.2 (NGC 7753) and 14.3 (NGC 7752) as given by Nilson (1973).

4. COMPARISON WITH OTHER INTERACTING GALAXIES

It is intersting to compare Arp 86 with other interacting galaxies in order to address its peculiarity while interpreting its evolutionary history. Star formation indices Hα and infrared flux show that global star formation activity in NGC 7753 is

slightly increased compared with that of field galaxies, whereas NGC 7752 is extremely active. The star formation rates per unit area for NGC 7752 and NGC 7753 are $1.68 \times 10^{-7}\ M_\odot$ yr^{-1} pc^{-2} and $2.23 \times 10^{-9}\ M_\odot$ yr^{-1} pc^{-2} (Laurikainen & Moles 1989), NGC 7752 being one of the most active galaxies found among interacting galaxies (compare with Fig. 1 in Bushouse 1987; notice that he uses $H_0 = 75$ km s^{-1} Mpc^{-1}, whereas we use $H_0 = 100$ km s^{-1} Mpc^{-1} here and throughout this paper).

Starburst galaxies have spectra that typically peak in the far-infrared and have a steep rise in the near-infrared. Spectra of this type are characteristic for thermal reradiation from dust grains. Far- and near-infrared fluxes are thus good indices of star formation, at least for such starburst galaxies with extended emission as NGC 7752, where the effect of cirrus emission is expected to be negligible. The far-IR/Hα ratio, 610 for Arp 86 (Laurikainen & Moles 1989), indicates a strong star formation rate, a large dust content, or both. For comparison the mean value for interacting galaxies in Bushouse's (1987) sample is 470. However, the far-IR apertures for Arp 86 covered both galaxies at 60 and 100 μm, in which wavelengths the main far-IR flux originates, so that the components cannot be distinguished.

Near-IR properties of M51-type galaxies have been compared by Joseph et al. (1984). The advantage of their study was that the infrared fluxes were possible to measure individually for both galaxies. They found that in five of the six cases studied, including Arp 86, the $K-L$ value is larger for the companion than for the main galaxy. It is worth noticing that NGC 7752 is much more active than any other companions of M51-type galaxies or interacting galaxies in the sample of Joseph et al., whereas NGC 7753 shows typical M51-type main galactic activity. In their paper Joseph et al. prefer reradiation from dust as the principal explanation for the red $K-L$ color, and discuss at length why other mechanisms such as free-free emission, nonthermal emission, or extinction cannot be the cause of the observed high $K-L$ values.

One reason for the extremely strong activity in NGC 7752 might be its large gas content. However, Jackson et al. (1987) found an interesting result: H I gas mass normalized to the total mass is found to be the same for normal spirals by Shostak (1978) as well as for starburst galaxies by Balzano (1983). The result of Jackson et al. suggests that in the majority of cases starburst galaxies need no excess gas to produce their activity, although it is not clear whether the same holds true for the extreme end of the luminosity function of starburst galaxies. For example, Balzano excluded very peculiar galaxies from her sample (typical Arp pairs). To be able to compare the gas masses of Arp 86 with those obtained by Jackson et al., we need first to calculate the total masses.

The total masses can be estimated using the rotation curves obtained by Marcelin et al. (1987). Adopting the maximum observed rotation amplitude of 165 km s^{-1} and inclination of 40° for the main galaxy, this yields the rotation amplitude 250 km s^{-1}. Using a relation appropriate for spherical mass models, estimating the mass within the radius 100″ from the center, and adopting a distance of 52 Mpc, we find that these numbers yield the mass $M(\mathrm{tot}) = 3.92 \times 10^{11}\ M_\odot$ for NGC 7753. For NGC 7752 we use the inclination 55°, in which case the inclination-corrected maximum rotation amplitude is 150 km s^{-1}, and the corresponding mass within 30″ radius is $3.96 \times 10^{10}\ M_\odot$. Marcelin et al. give the corresponding masses 1.6×10^{11} and $2.4 \times 10^{10}\ M_\odot$, considerably smaller than our values. The reason for the difference is that for the companion we used a larger galaxy radius than they did, based on the visual inspection of our images, and for the main galaxy a larger maximum rotation amplitude and smaller inclination were adopted by us. The maximum rotation amplitude was used (thus assuming an initially flat rotation curve to the edge of the disk), because the observed decrease in the outer parts of the rotation curve was assumed to be an effect caused by the tidal perturbation. Evidence for this is given in Paper II.

The neutral hydrogen masses for NGC 7752 and NGC 7753 are $4.7 \times 10^9\ M_\odot$ (Jackson et al 1987), and $1.65 \times 10^{10}\ M_\odot$ (Davis & Seaquist 1983; Krum & Salpeter 1980; Staveley-Smith & Davies 1987), the latter being the mean value of the three measurements. Normalizing these values to the total masses, gas–to–total-mass ratios 0.12 (NGC 7752) and 0.04 (NGC 7753) are obtained. For NGC 7752 Jackson et al. give a gas–to–total-mass ratio of 0.2, based on a smaller radius in their mass estimation. Comparing these ratios with the mean values obtained for normal spirals (0.06) and starburst galaxies (0.07), we can see that the gas content in NGC 7753 is normal, whereas in NGC 7752 it is abnormally large.

To make the gas content normal in NGC 7752, it should be reduced by a factor of 1.7. If this gas, $2.0 \times 10^9\ M_\odot$, is added to the main galaxy, its $M(\mathrm{H\ I})/M(\mathrm{tot})$ would be increased only from 0.042 to 0.047. If the original gas content in NGC 7753 were 0.07 instead of the observed value 0.04, NGC 7753 must have lost $2.75 \times 10^{10}\ M_\odot$ of its gas, which is almost 6 times the actual gas mass in NGC 7752. According to these calculations it is clear that even if NGC 7752 received all its excess gas from the main galaxy, it would hardly affect the normalized gas fraction in the main galaxy.

For the lack of observations it is difficult to compare the gas content of Arp 86 with those of other M51-type objects. However, the companion of M51 is known to be almost devoid of H I gas, and neutral gas was not detected by Davis & Seaquist (1983) for other companions of M51-type objects.

The mass-to-luminosity ratio is a useful way to parameterize the mass associated with star formation activity and thus to estimate the gas consumption time scale. Wright et al. (1988) calculated the ratio of the nuclear mass to total IR luminosity for a sample of interacting galaxies, obtaining the mean value of 0.08. IR luminosities were used, because for the galaxies under discussion the bolometric luminosities are dominated by IR emission. The luminosities were estimated from the 10 μm fluxes using the approximation $L_{\mathrm{IR}} = 15 L_{10}$ by Scoville et al. (1983), and masses were calculated within the same apertures used to measure IR fluxes. Calculating the mass-to-luminosity ratio for NGC 7752 in the same way, we obtained $M/L_{\mathrm{IR}} = 0.18$. This is only an estimate, because in reality the IR emission in NGC 7752 is more extended than the aperture size used in the IR measurements. The minimum mass-to-light ratio which can be maintained by thermonuclear energy generation over a Hubble time is around unity, so that low M/L_{IR} ratios are indicative of significant recent star formation. The rather high mass-to-luminosity ratio obtained for NGC 7752 as compared with the values obtained by Wright et al. for interacting galaxies is in agreement with the fact that the galaxy seems not to have any active nucleus.

The mass-to-luminosity ratio can be used to estimate the gas consumption time scale. Again we follow the method of Wright et al. (1988). We consider the formation of OBA stars with a constant star formation rate that has proceeded for a sufficiently long time so that equilibrium has been established between

the death and birth rates of massive stars. In starburst galaxies the lower cutoff of the Miller-Scalo initial mass function is assumed to be high, the mass range 1.6–60 $M_\odot$ being adopted. It is assumed that massive stars return 75% of their mass to the interstellar medium and that 10% of the total mass is in gas. This way we get the maximum duration of the starburst $T = 1.1 \times 10^8$ yr, which is among the values obtained by Wright et al. for interacting galaxies, being typically 1×10^7–2×10^8 yr. In reality the gas content in NGC 7752 is 20% (or higher if molecular gas is included), which would increase the maximum duration of the starburst by a factor of 2. Because of the extremely large activity and the large gas content, it is tempting to argue that the small galaxy must be continuously fed by the main galaxy (see Paper II). This feeding process cannot be extremely violent however, because Durret & Warin (1990) found that the ratio between the FWHM of the ionized gas and the maximum rotation amplitude is nearly unity, indicating that gas turbulent motions are not very significant.

5. CONCLUSIONS

The following conclusions can be summarized:

1. Initial observational parameters for dynamical modeling of Arp 86 were determined. The inclination was found to be 40° for the main disk and 55° for the companion galaxy. The mass distribution for NGC 7753 follows the $R^{1/4}$ law inside the inner 15″ from the center, whereas in the range 15″–60″ it is exponential with a scale length of ≈20″. For the companion galaxy the intensity distribution is consistent with an exponential disk for the radius 5″–15″ with a scale length of 3.″1–3.″7, depending on the wavelength, covering approximately the active part of the galaxy, whereas in the innermost 5″ the intensity drops rapidly, possibly due to absorption. The outer disk of NGC 7752 is extended and contains more mass than implied by the exponential model.

2. The tidal bridge was found to be bluer than the tail in $B-V$, and $B-R$ as well as in $V-R$. The bridge manifests extremely blue $B-V$ color near the companion galaxy, thus indicating ongoing star formation processes. The bridge also has a strong $V-R$ gradient, which is suggested to be induced by long-term stellar formation processes.

3. Locations and distributions of star-forming regions vary along the spiral arms. At the end of the bridge there are large star-forming complexes following the double bridge arms; in the inner parts of the tidal arms star formation is concentrated to the concave edges of the arms, whereas in the disk within the radius of 35″ from the center, star formation is again clumpy and distributed within the whole arm width.

REFERENCES

Arp, H. 1969, A&A, 3, 418
Balzano, V. A. 1983, ApJ, 268, 602
Burstein, D., & Heiles, C. 1982, AJ, 87, 1165
———. 1984, ApJS, 54, 33
Bushouse, H. A. 1987, ApJ, 320, 49
Davis, L. E., & Seaquist, E. R. 1983, ApJS, 53, 269
de Vaucouleurs, G., de Vaucouleurs, A., & Corwin, H. G., Jr. 1976, Second Reference Catalog of Bright Galaxies (Austin: Univ. Texas Press)
Durret, F., & Warin, F. 1990, A&A, 238, 15
Elmegreen, D. M., & Elmegreen, B. G. 1987, ApJ, 314, 3
Hernquist, L. 1990, in Dynamics and Interactions of Galaxies, ed. R. Wielen (Berlin and Heidelberg: Springer-Verlag), 108
Jackson, J. M., Barret, A. H., Armstrong, J. T., & Ho, P. T. P. 1987, AJ, 93, 531
Joseph, R. D., Meikle, W. P. S., Robertson, N. A., & Wright, G. S. 1984, MNRAS, 209, 111
Krum, N., & Salpeter, E. E. 1980, AJ, 85, 1312
Landolt, A. U. 1983, AJ, 88, 439
Larson, R., & Tinsley, B. 1978, ApJ, 219, 49
Laurikainen, E., & Aparicio, A. 1993, in preparation
Laurikainen, E., & Moles, M. 1989, ApJ, 345, 176
Marcelin, M., Lecoarer, E., Boulesteix, J., Georgelin, Y., & Monnet, G. 1987, A&A, 179, 101
Mirabel, I. F., Dottori, H., & Lutz, D. 1992, A&A, 256, L19
Nilson, P. 1973, Uppsala General Catalogue of Galaxies (Uppsala Astron. Obs. Ann., Vol. 6)
Petrov, G. T. 1986, Ap&SS, 124, 407
Salo, H., & Laurikainen, E. 1993, ApJ, 410, 586 (Paper II)
Savage, B. D., & Mathis, J. S. 1979, ARA&A, 17, 73
Schombert, J. M., Wallin, J. F., & Struck-Marcell, C. 1990, AJ, 99, 497
Scoville, N. Z., Becklin, E. E., Young, J. S., & Capps, R. W. 1983, ApJ, 271, 512
Shostak, G. S. 1978, A&A, 68, 321
Staveley-Smith, L., & Davies, R. D. 1987, MNRAS, 224, 953
Toomre, A., & Toomre, J. 1972, ApJ, 178, 623
Vorontsov-Vel'yaminov, B. A. 1958, Soviet Astron., 1, 9
———. 1976, Soviet Astron., 19, 422
Wright, G. S., Joseph, R. D., Robertson, N. A., James, P. A., & Meikle, W. P. S. 1988, MNRAS, 233, 1
Zwicky, F. 1956, Ergebn. Exakten Naturw., 29, 344

1993ApJ...410..574L

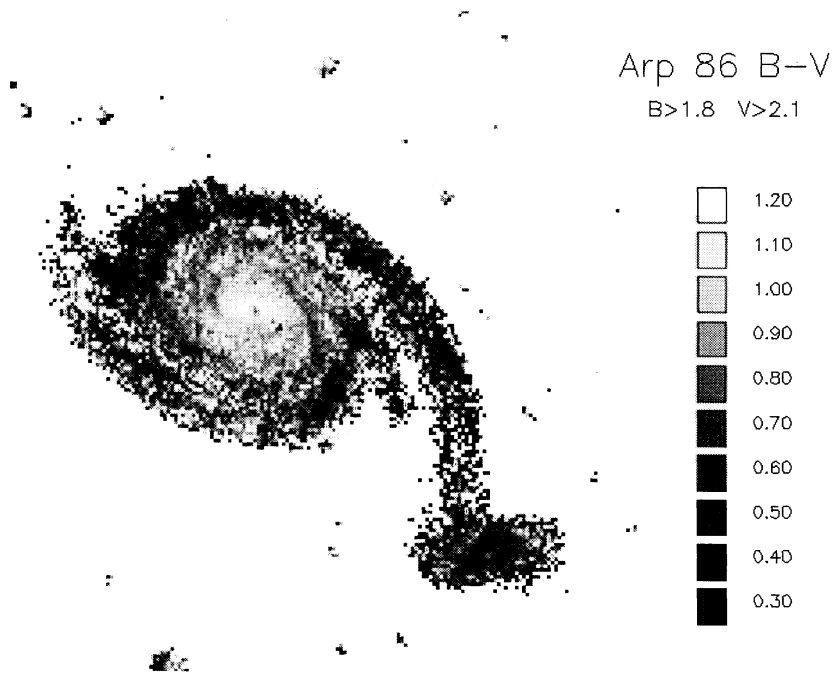

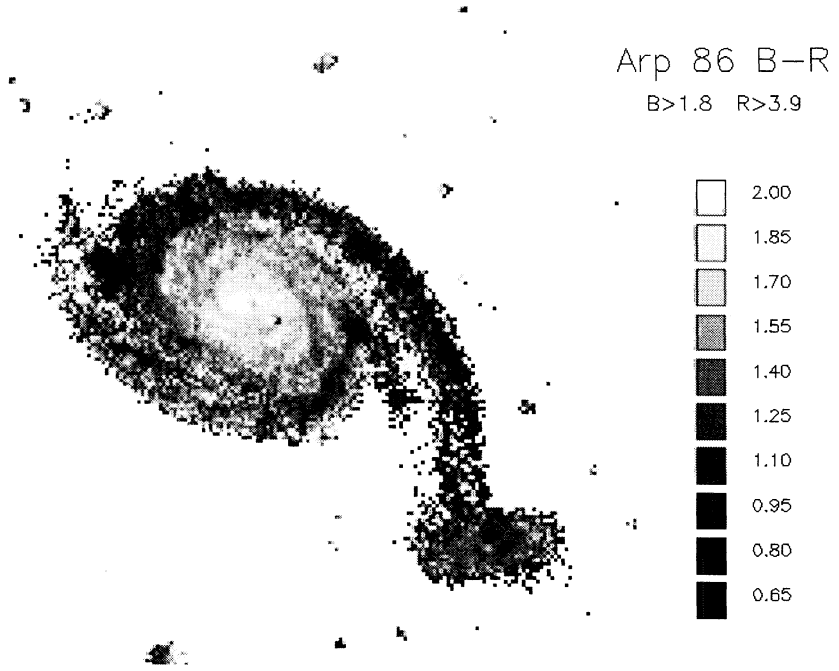

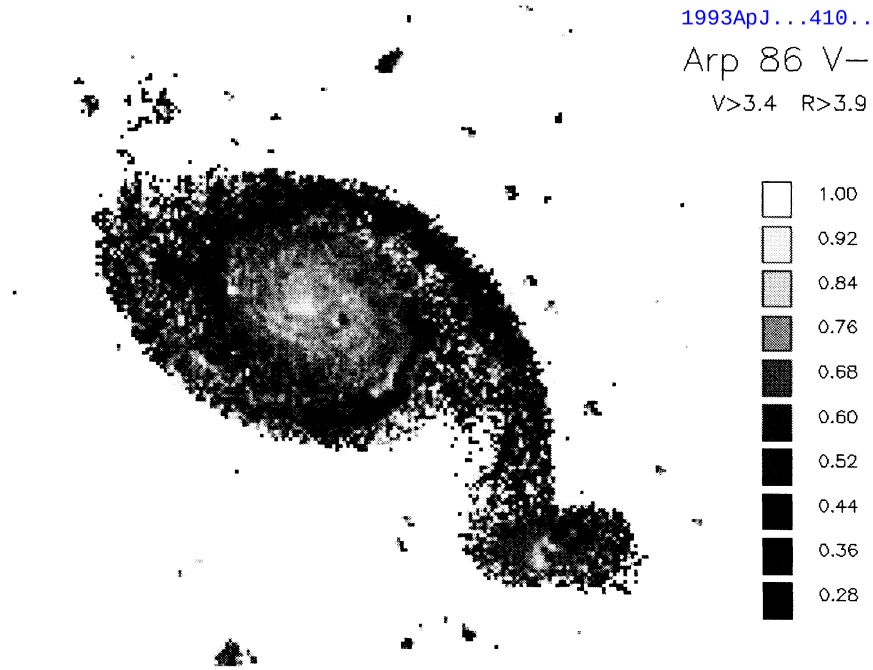

FIG. 8.—Color index maps in $B-V$, $V-R$, and $B-R$. The method of constructing the maps is explained in the text. The limits for B, V, and R indicate the minimum accepted ADU levels in the rebinned images, corresponding to values 3 σ above the sky noise level.

LAURIKAINEN, SALO, & APARICIO (see 410, 580)

PLATE 4